PINSA, **66, A,** No. 2, March 2000, pp. 177 – 197

ULTRAFAST ELECTRON TRANSFER DYNAMICS IN SENSITIZED TiO_2 NANOPARTICLES

HIRENDRA N GHOSH, JOHN B ASBURY, AND TIANQUAN LIAN*

Department of Chemistry, Emory University, Atlanta, GA 30322, (USA)

(Received 14 July 1999; Accepted 09 September 1999)

We have studied electron transfer dynamics between TiO_2 nanoparticles and molecular adsorbates using femtosecond mid-infrared spectroscopy. We have demonstrated that dynamics of the injected electrons in TiO_2 could be directly monitored through their mid-IR absorption and those of the adsorbates could be measured by their vibrational spectral change. $Ru(dcbpy)_2(NCS)_2$ (dcbpy=2,2′-bypyridine-4,4′-dicarboxylate) sensitized TiO_2 nanocrystalline films were studied as a model system for ultrafast electron injection from the excited state of the sensitizer to nanoparticles. Optical excitation of the MLCT band at 400 nm promotes an electron from a filled Ru d orbital to the π^* orbital of the dcbpy ligand. The subsequent electron injection to TiO_2 was found to occur with a time constant of *ca* 50 fs by directly measuring the transient IR absorption signal of the injected electrons in TiO_2. These injection dynamics are as fast as, if not fast than, the electronic or vibrational relaxation within the excited states. Back electron transfer from nanoparticles to the adsorbates was studied in interfacial charge transfer complexes formed by $Fe(II)(CN)_6^{4-}$ and TiO_2 colloidal nanoparticles. Optical excitation at 400 nm directly promotes an electron from $Fe(II)(CN)_6^{4-}$ to TiO_2 as indicated by the measured instrument-response-function limited appearance time of transient IR signal. The back electron transfer time from TiO_2 to $Fe(III)(CN)_6^{3-}$ was measured by the bleach recovery of CN stretching mode. A highly non-single-exponential recombination process was observed and was tentatively attributed to different recombination rates for injected electrons trapped at different sites in TiO_2. The measured decay of the IR absorption of electrons can be attributed to back electron transfer and electron trapping. Since the back electron transfer kinetics can be measured independently, the trapping dynamics can be determined. Electron trapping dynamics in a bulk crystal and nanocrystalline thin films were found to be similar in the first nanosecond, showing a >> 1 ns decay time. Trapping dynamics are much faster in the colloidal nanoparticles, indicating a much higher trap state density.

Key Words: Ultrafast Electron Transfer Dynamics; Nanoparticles; Femtosecond Spectroscopy; Solid-Liquid Interface; Relaxation Dynamics; Molecular Adsorbates

1 Introduction

Electron transfer (ET) between molecular adsorbates and semiconductor nanoparticles has been a subject of intense research interests[1-3]. The understanding of this fundamental process is essential for the application of semiconductor nanoparticle materials in photography[4], solar energy conversion[5], waste degradation[6], and nano-scale devices[7]. For example, photoelectrochemical solar cells based on dye sensitized nanocrystalline TiO_2 thin films[8] have received much attention in recent years because of their potential applications as a cost effective alternative to silicon based cells[1-3,9,10]. Gratzel's group reported that solar cells based on $Ru(dcbpy)_2(NCS)_2$ [dcbpy=(4,4′-Dicarboxy-2,2'-Bipyridine)] (or Ru N3) sensitized nanocrystalline TiO_2 thin films could achieve a solar to electric power conversion efficiency of about 10%[8,11]. The high conversion efficiency can be attributed to high solar energy harvesting by the sensitizer and high photon to current conversion efficiency. A schematic of various processes in dye sensitized semiconductor nanomaterials is shown in Fig. 1. A high photon to current conversion efficiency requires a fast electron injection rate from the sensitizer to the semiconductor and a much slower back electron transfer rate to the sensitizer[9].

Unlike in homogeneous solutions[12-14], electron

*To whom correspondence should be addressed. tlian@emory.edu

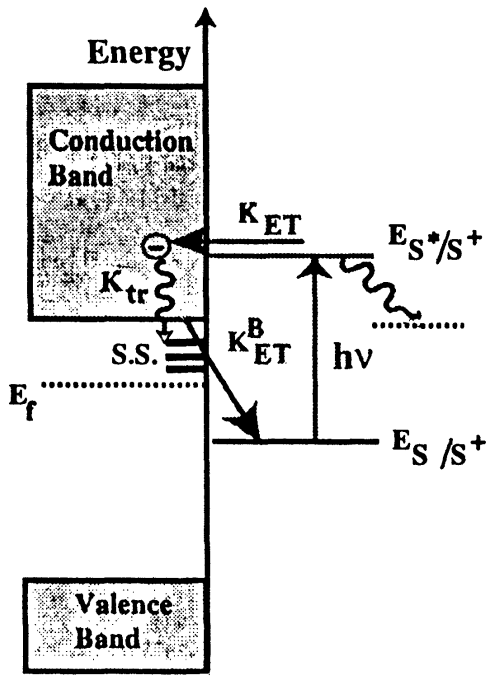

Fig. 1 A schematic of interfacial electron transfer

transfer dynamics in the solid-liquid interface[15-18] are still poorly understood[1,2,19]. The interfacial nature of these processes has hindered the theoretical and experimental studies in the past. In the solid, electrons can be delocalized in the continuous electronic levels that form the conduction band, or they can be localized on the surface or in trap states. The exact nature of the states that couple to the adsorbates is still unclear. Experimentally, the study of bulk surface often demands sophisticated surface science methods in UHV chambers[20]. Studies of adsorbates on semiconductor or metal surfaces by these techniques have gained great insights into small molecule/solid interaction. Ultrafast time resolved techniques have also been applied to study dynamical processes on well-defined surfaces[20-25]. Although they may be over simplified models for the solid-liquid interface, the detailed knowledge of these systems is crucial for understanding electron transfer process in the bulk solid/liquid interface. Most of the previous understanding of interfacial charge transfer is derived indirectly from steady-state photocurrent measurements in electrochemical cells[1,19,26-28]. Unfortunately, obtaining ET rates from steady state photocurrent is often quite complicated because the latter depends on many other interface and bulk properties in addition to the interfacial ET rates[1,19]. Time-resolved photoluminescence measurements have also been used successfully to obtain electron transfer dynamics in the solid-liquid interface of strongly luminescence semiconductor electrodes[29-31]. Efforts in developing *in situ*, direct and interface specific spectroscopic techniques for studying interfacial ET have resulted in some elegant yet complicated techniques, such as sum frequency (SFG) and second harmonic (SHG) generation[32-34], and surface restricted grating techniques[35].

In recent years, there has been a rapid development in the synthesis and characterization of nanometer size metal and semiconductor particles. In addition to their fascinating properties resulting from quantum size confinement, the large surface area and small size of these materials also enable the study of their properties by time-resolved absorption techniques. The surface chemistry of these materials can be readily studied without sophisticated surface science techniques and in more realistic environments. Although it is still unclear whether the knowledge of the nanoparticle/liquid interface can be applicable to the bulk/liquid interface, the understanding of nanoparticle/liquid interface is important in its own right. The operation of most devices based on this new class of materials is directly related to the charge transfer dynamics in and out the nanoparticles and carrier relaxation/combination dynamics within the nanoparticles. For this reason, photophysics of and carrier relaxation and recombination dynamics in metal and semiconductor nanoparticles have been actively studied in recent years[36-41]. Interested readers can refer to review articles[36,38,39] for more details on that subject. In this article, we will focus on ultrafast interfacial charge transfer between semiconductor nanoparticles and molecular adsorbates. In recent years there have been many studies of electron transfer dynamics in dye sensitized semiconductor nanoparticles and thin films using time-resolved laser spectroscopy[35,42-56]. By measuring the excited state dynamics of the sensitizer through transient absorption[46-48,55] or fluorescence decay[49,56], the electron injection rates from various adsorbed dye molecules into various semiconductor nanoparticles have been determined[35,46-49,55,56], ranging from subpico-

seconds[43,48-50], to 10's of picoseconds[57], and even nanoseconds[58]. Back ET times were often measured by monitoring the bleach recovery of the ground state absorption. Although much insight into interfacial ET has been gained through these studies, transient absorption studies in the visible and near IR region are often hindered by spectral overlap of absorptions in various electronic states, such as the excited, oxidized, and ground states, as well as stimulated emission. Fluorescence quenching studies can sometimes be complicated by non-ET related quenching pathways, such as energy transfer among sensitizer molecules[45,51], and the dynamic fluorescence Stokes shift[56]. Because of these complexities, a systematic study of the dependence of interfacial ET rates on various adsorbate/nanoparticle properties has not been achieved.

In order to systematically study ET dynamics in the solid-liquid interface, new *in situ* techniques that are capable of assigning the ET process unambiguously and that complement the existing visible/near-IR transient absorption and fluorescence quenching techniques are needed. Femtosecond mid-IR spectroscopy[59] provides such an approach for these interfacial problems because it can directly study the dynamics of electrons in the semiconductor in addition to the dynamics of the adsorbates. As demonstrated in bulk[60,61] and quantum well[62] semiconductor materials, valence band holes and conduction band electrons in semiconductors have strong absorptions in the infrared region. These absorptions consist of Free Carrier Absorption[63], which is often broad and increases with wavelength, Intra-Band Transitions[63] between different valleys (or subbands) within the conduction or the valence bands, as well as absorptions of trap states. Since these IR absorptions of electrons are direct evidence for the arrival of electrons inside semiconductors, they provide an unambiguous spectroscopic probe for studying interfacial electron transfer between semiconductors and adsorbates. Furthermore, unlike fluorescence quenching, femtosecond mid-IR spectroscopy is a general technique. It can be used for any adsorbate/nanoparticle system, allowing a systematic study of the dependence of ET rates on the properties of the adsorbates, semiconductors and the solvent environments. It should be pointed out that injected electrons in semiconductors could also absorb in the near IR region. Near-IR probed of electron injection dynamics have been reported[43,44]. However, in the near IR region, it may be difficult to avoid the spectral overlap with the electronic transitions of large dye molecules[64], which is not a problem in the mid-IR region. Injected electrons can also be probed in the far IR and microwave region. Direct measurement of microwave absorption of injected electrons in dye sensitized nanocrystalline thin films has been demonstrated in the nanosecond time scale[58]. Ultrafast THz spectroscopy[65-67] should provide another convenient probe for ultrafast electron injection dynamics.

Recently, transient mid-IR spectroscopy was used to study electron transfer in sensitized nanoparticles by Heilweil's group in NIST[42,68] and us[42,64,69-71]. This technique can directly probe the mid-IR absorption of electrons inside semiconductors without the complication of broad electronic transitions of the adsorbates. We have applied this approach to TiO_2 nanoparticles sensitized with $Ru(dcbpy)_2(SCN)_2$ and related compounds[64,70,72], coumarin 343[69] and related organic dyes and even smaller ions such as $Fe(II)(CN)_6^{4-}$[71] and SCN^-[73]. The ability to study small adsorbates allows for more detailed and quantitative study of interfacial ET dynamics. In this paper, we will give an overview of our recent studies of interfacial electron transfer between TiO_2 nanoparticles and molecular adsorbates. This paper is not intended as a comprehensive review on interfacial electron transfer on TiO_2 nanoparticles, although relevant comparisons with closely related works are made. The paper is organized as follows.

In Section 2, the experimental technique used for this study is described. The results and discussions are presented in Section 3. We will start out with the assignment of the transient mid-IR absorption in TiO_2. Electron transfer dynamics in Ru N3 sensitized TiO_2 nano-films will be discussed with emphasis on electron injection dynamics. The electron transfer dynamics in TiO_2/Fe(CN)6 complex will be analyzed as a model for back electron transfer from TiO_2 to $Fe(III)(CN)_6^{3-}$. A discussion of the electron relaxation dynamics in bulk crystal, nano-films and nanoparticles will also be presented.

2 Experimental Section

Femtosecond Tunable Spectrometer

The femtosecond tunable visible and infrared spectrometer used for this study is based on a regeneratively amplified femtosecond Ti:Sapphire laser system from Clark-MXR (1KHz repetition rate at 800 nm, 100 fs, 900 μJ/pulse), and nonlinear frequency mixing techniques as shown in Fig. 2. The 800 nm output pulse from the regenerative amplifier is split into two parts to generate pump and probe pulses. One part, with 300 μJ/pulse, is frequency doubled and tripled in BBO crystals to generate pump pulses at 800, 400 or 267 nm.

IR Probe

In the IR probe experiments, the remaining 600 μJ of the 800 nm pulse is used to pump a Clark IR Optical Parametric Amplifier to generate two tunable near IR pulses from 1.1 to 2.5 μm. These signal and idler pulses are combined in a $AgGaS_2$ crystal to generate mid-IR pulses from 3 to 10 μm by difference frequency generation. The mid-IR pulses have a typical intensity fluctuation of 1 to 3%. The probe IR pulses are divided into a signal and reference beam. While the signal beam measures the absorption of the sample, the reference beam is used to normalize the laser intensity fluctuations. These probe beams are vertically displaced and dispersed in a monochromater, from which a 2 to 3 cm^{-1} slice of the total spectrum (approximately 200 cm^{-1}) is measured by a pair of Mercury Cadmium Telluride (MCT) detectors. To minimize low frequency laser fluctuations, the main noise source, every other pump pulse is blocked with a synchronized chopper (New Focus model 3500) at 500 Hz, and the absorbance change is calculated with two adjacent probe pulses (pump blocked and pump unblocked). About 4% of the chopped pump beam is split by a beam splitter and detected in a photodiode (Thorlab PDA 50) to monitor the intensity of the pump beam and phase of the chopper (pump blocked *vs.* unblocked). The output from the MCT detectors and the photodiode are integrated in three separate gated boxcar integrators (Stanford Research Systems SR 250), digitized in a 12 bit A/D converter (National Instrument AT-MIO-64E-3), and recorded by a Pentium PC for each laser pulse. The typical noise in the measured absorbance change is about 0.4 to 0.8% for every pair of laser pulses. Transient absorption spectra are recorded by scanning the monochromater at fixed delay times, and the kinetics traces at fixed wavelengths are recorded by scanning the delay time. The zero delay time and instrument response for a 400 nm pump/ mid-IR probe experiment are determined in a thin silicon wafer or thin film of TiO_2 nanoparticles, in which absorption of 400 nm photons lead to the instantaneous generation of charge carriers that absorb strongly in the mid-IR region[63]. The typical

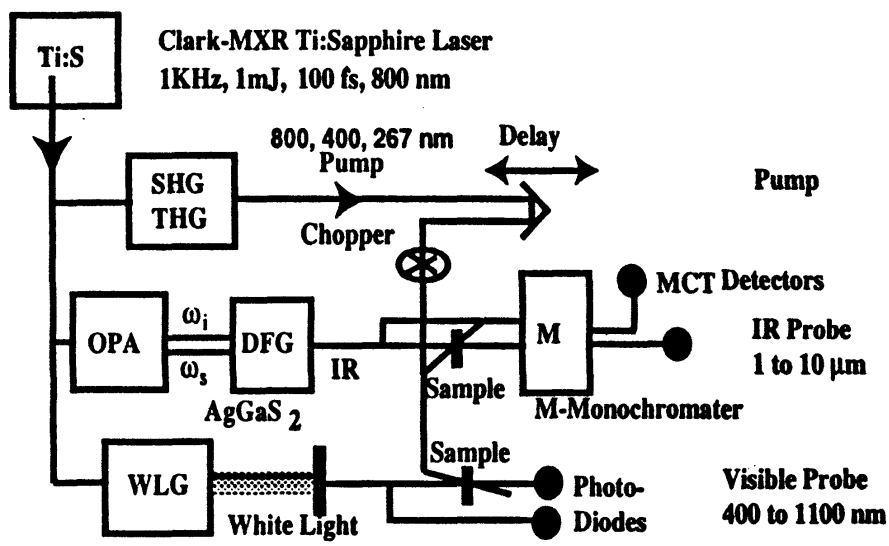

Fig. 2 A schematic of the tunable femtosecond spectrometer

instrument response, which is determined in every experiment, can be well presented by a Gaussian function with FWHM ranging from 150 to 320 femtosecond.

Visible Probe

To generate visible probe pulses, about 6 μJ of the 800 nm beam is focused onto a 2 mm thick sapphire window. The intensity of the 800 nm beam can be adjusted by iris size and ND filters to obtain a stable white light continuum in the 430 nm to over 1000 nm region. A variable interference filter (from Optical Coating Laboratory Inc.) selects approximately 10 nm slices of the white light to provide tunable probe pulses. The probe pulses are split into the signal and reference beams, which are detected by two matched photodiodes with variable gain (PDA50 from Thorlabs Inc.). The noise level of the white light is about 0.4% with occasional spikes due to fluctuations in the oscillator output. We have noticed that most laser noise is low frequency noise and can be eliminated by comparing the adjacent probe laser pulses (pump blocked vs. unblocked) similar to the IR setup. The typical noise in the measured absorbance change is about 0.1 to 0.2%. Additional laser intensity normalization with the signal and reference beams is often found to be unnecessary.

Materials

Synthesis of TiO_2 Nanoparticles

Nanometer sized TiO_2 was prepared by controlled hydrolysis of titanium(IV) tetraisopropoxide[74]. 100 ml solution of $Ti[OCH(CH_3)_2]_4$ (Aldrich, 97%) dissolved in isopropyl alcohol (5:95) was added dropwise (1ml/min) to 900 ml of doubly distilled water (2°C) at *p*H 1.5 (adjusted with HNO_3). The solution was continuously stirred for 10-12 hours until a transparent colloid was formed. Both titanium(IV) tetraisopropoxide and isopropyl alcohol were purified by distillation. The colloidal solution was concentrated at 35-40°C with a rotary evaporator and then dried with a nitrogen stream to yield a white powder. The estimated size of the particles is ca. 5 nm.

Preparation of $Fe(II)(CN)_6^{4-}$ Sensitized TiO_2 Nanoparticles

TiO_2 nanoparticle powder was dissolved in D_2O solution to obtain colloidal solution of 10g/L concentration. The colloid was protected by 10g/L polyvinyl alcohol (PVA) and kept at *p*H 2 by adding 10^{-2} M of $HClO_4$. The colloidal solution was then mixed with $K_4Fe(CN)_6$ (25 mM), and kept in the dark and in N_2 atmosphere. After stirring for >10 hours, a deep orange coloured solution was formed and remained stable for a few days. The visible absorption is attributed to a charge transfer complex formed between $Fe(CN)_6^{-4}$ and TiO_2 nanoparticles. The optical density of the solution in a 100 μm thick cell was about 0.3 at 400 nm. The unsensitized TiO_2 colloidal solution sample used in the experiment had no noticeable absorption at 400 nm. D_2O was used instead of H_2O to improve the transmission in the 1900 to 2200 cm^{-1} region.

Film Sample Preparations

Concentrated TiO_2 nanoparticle colloids were first prepared as previously described, using Degussa P25 TiO_2 (about 70% anatase and 30% rutile) as the starting material[11]. Thin films were prepared using these colloids according to a published procedure[64]. The films were prepared on c-cut polished sapphire substrates and fired at 450°C for 45 minutes in air. TiO_2 films were 5 μm thick with good transparency. The Al_2O_3 films were ~15 μm thick and showed greater scattering than the TiO_2 films. Immersion and storage of the TiO_2 and Al_2O_3 films in a room temperature ethanol solution containing 200 μM Ru N3 and 20 mM chenodeoxycholic acid resulted in adsorption of the Ru N3 to the porous film surface. The resulting dye-sensitized films showed an absorbance of ~1.0 at 400 nm and 550 nm. The absorbance at 400 nm for a typical naked film used in the experiment was about 0.3 OD with contributions from both absorption and scattering of the nanocrystalline films. High purity Ru N3 was purchased from Solaronix (Lausanne, Switzerland).

3 Mid-IR Absorption of Electrons in TiO_2

The mid-IR absorption of free carriers in many different semiconductor materials has been reported[63]. Reduced rutile TiO_2 crystals were also found to have significant absorption in the mid-IR region due to excess electrons in the conduction band[75]. There has not been any careful characterization of mid-IR absorption of electrons

in TiO_2 nanoparticles. Since electrons can be generated through excitation of the bandgap transitions in unsensitized nanomaterials or injection from dye-sensitizers, their IR absorption spectra can be characterized by transient IR spectroscopy. We have observed mid-IR absorption signals of electrons in or trapped below the TiO_2 conduction band generated by both approaches.

For the rutile type TiO_2 crystals, whose bandgap is around 3.02 eV (or 413 nm)[75], optical excitation at 400 nm leads to the generation of electrons in the conduction band and holes in the valence band. The absorption of these carriers was characterized by measuring the transient IR signal in the mid-IR region before the recombination of electrons and holes. Shown by the connected open circles in Fig. 3 is the transient IR signal in the 5 μm (2000 cm^{-1}) region for a rutile TiO_2 crystal at 3 ps after 400 nm excitation. This signal is very broad and is present in the mid-IR region from 1700 to 2400 cm^{-1}, although the detailed structure is yet to be carefully characterized. The typical mid IR absorption spectra of electrons in many semiconductor materials are broad consisting of Free Carrier Absorption, Intraband Transitions, and trap states[63]. While the observed IR signal shown in Fig. 3 is consistent with the broad IR absorption of electrons, the assignment of the relative contributions of different transitions to the observed signal is not possible due to the very small spectral region studied so far. The rise time of the signal in the bulk TiO_2 crystal is instrument response time limited[69], as shown in Fig. 5, consistent with a direct generation of electrons and holes by the excitation pulse. The decay of the signal within the first nanosecond is characterized by a pulse width limited decay, shown in Fig. 5, and a subsequent slow decay of the amplitude with a time constant >> 1 ns as shown in Fig. 14. Also shown in Fig. 3 (the connected full circles) is the transient IR signal in the nanocrystalline thin film at 3ps after 400 nm excitation. Again similar broad IR features are observed for electrons and holes. Here direct excitation into trap states near the band edge may be responsible for the absorption at 400 nm.

Similar broad transient mid-IR absorption for injected electrons can also be observed in sensitized nanoparticles. Shown in Fig. 4 are transient IR spectra of coumarin 343 (C-343) sensitized TiO_2 nanoparticle colloidal solution after 400 nm excitation. C-343 sensitized TiO_2 nanoparticles have been shown to undergo efficient electron injection from the C-343 excited state to TiO_2 conduction band upon photo-excitation of the dye[49,76]. Using fluorescence up-conversion technique, forward electron injection time of 180± 50 fs was inferred from the fluorescence decay time of C-343 in a colloidal solution of sensitized TiO_2 nanoparticles in H_2O (with 5% acetone)[49].

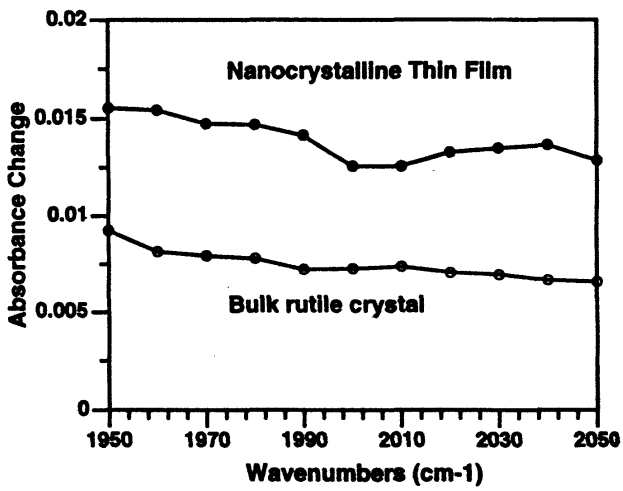

Fig. 3 Transient mid IR absorption in a bulk rutile TiO_2 crystal (open circles) and nanocrystalline TiO_2 thin film at 3 ps after 400 nm excitation

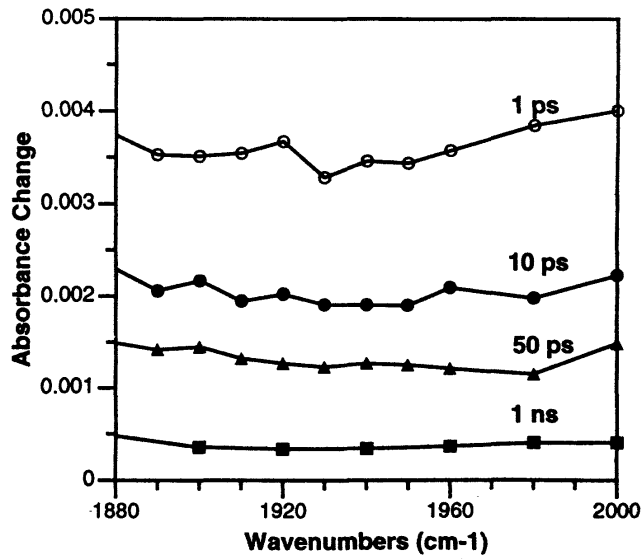

Fig. 4 Transient mid IR absorption C343 sensitized colloidal TiO_2 nanoparticles at 1, 10, 50 and 1000 ps after 400 nm excitation. The absorption is assigned to injected electrons in TiO_2.

While the broad absorption feature shown in Fig. 4 is a typical signature of electrons in semiconductor, this assignment is further confirmed by the lack of similar signals in blank samples of C-343 molecule in ethanol, D_2O solvent, and unsensitized TiO_2 nanoparticles in D_2O[69].

Since the mid-IR absorption is a direct probe of injected electrons, the rise time of the signal should correspond to the electron injection time. The kinetics trace for C-343 sensitized TiO_2 nanoparticles at 2000 cm^{-1} is shown by the full circles in Fig. 5. We have subtracted a small solvent background absorption signal at around t=0[69]. The rise time of the observed signal can be well fit by convolution of a single exponential rise and the instrument response function, represented by a Gaussian function with 160 fs FWHM. The solid line in Fig. 5 is a fit to the kinetics at 2000 cm^{-1} with a rise time constant of 135 fs. The best fit to the kinetics at 1900, 1950, and 2000 cm^{-1} yields time constants ranging from 100 to 150 fs. We therefore report an average rise time of 125 ± 25 fs. The risetime of the transient IR signal represents the formation time of electrons in TiO_2 through injection from the excited state of C-343. Our result is in agreement with other reported ultrafast injection times of 180±50 fs[49].

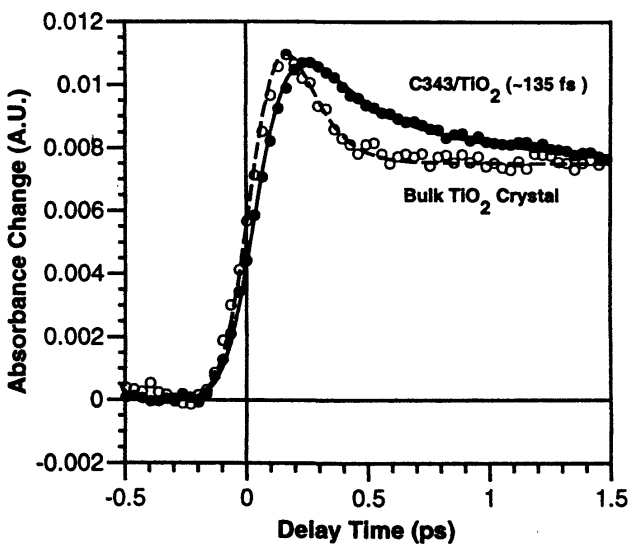

Fig. 5 Transient kinetics in C343 sensitized TiO_2 nanoparticles (full circles) probed at 2000 cm^{-1} after 400 nm excitation. The measured 135 fs rise time is attributed to the electron injection time from the excited state of c343 to TiO_2. Also shown is the kinetics trace in a bulk rutile crystal (open circles) at 1960 cm^{-1} after 400 nm excitation. Here the direct band gap excitation leads to instantaneous generation of electrons and holes.

This study demonstrated that injected electrons have strong mid-IR absorption that can be used to follow the injection kinetics. We have used this spectral signature to study electron transfer process between molecular adsorbates and semiconductor nanoparticles. It should be noted here that there is more information contained in the IR absorption signal that can be further obtained. Although the mid IR absorption spectra shown in Figs. 3 and 4 are very similar in the 5 μm region for these three different TiO_2 materials, the exact shape in a wider region has yet to be determined. The spectral dependence in a wider range should reveal the nature of the electrons, because trapped and free electrons may have very different spectral dependence. In addition, the time dependence of the IR spectra should contain information about electron relaxation (cooling and trapping) within the nanoparticles and back transfer to the adsorbates.

4 Ru N3 Dye Sensitized TiO_2 Thin Film : Ultrafast Electron Injection Dynamics

Since the report by Gratzel's group that solar cells based on $Ru(dcbpy)_2(NCS)_2$ [dcbpy=(4,4'-Dicarboxy-2,2'-Bipyridine)] (or Ru N3) sensitized nanocrystalline TiO_2 thin films can achieve a solar to electric power conversion efficiency of about 10%[8,11], electron injection and recombination properties of Ru dye sensitized semiconductors have been studied by many groups[42,43,48,51,58,64,68,70,77-86]. The exact nature and time scale of the electron injection step for Ru N3 has been a subject of a recent debate[43,48]. To unambiguously resolve the electron injection step, we have recently studied the Ru N3 sensitized TiO_2 thin film with femtosecond mid IR spectroscopy. We also investigated the photophysics of the sensitizer to compare the excited state relaxation and electron injection dynamics.

Photophysics of Ru N3 in Ethanol and on Al_2O_3

In order to understand the detailed electron injection dynamics of the Ru N3 sensitized TiO2 films, the excited state dynamics of the sensitizer

molecules themselves, without the complication of electron injection, need to be understood. We have studied the photophysics of Ru N3 1) in ethanol solution; and 2) adsorbed on Al_2O_3 film after 400 nm excitation. The band gap for Al_2O_3 is about 8 eV[87], and its conduction band is not accessible by the MLCT excited state of the sensitizer[84]. Thus this system should serve as a good model for the photophysics of the adsorbate.

Shown in Fig. 6 are transient IR spectra in the CN stretching mode region of Ru N3 in ethanol (connected full circles) and adsorbed in Al_2O_3 film (connected open circles) at 5 ps after 400 nm excitation. The excitation leads to bleach of the ground state absorption at 2115 cm^{-1}, while creating a new band at 2040 cm^{-1}. The bleach at 2115 cm^{-1} is identical to the peak of the CN stretching mode of freshly prepared Ru N3 in ethanol. The transient spectra in these two samples are almost identical except for the small shoulder at 2140 cm^{-1} and its corresponding excited absorption at 2075cm^{-1} that is present only in the ethanol solution[72].

In a previous study on $Ru(bpy)_3^{+2}$, it was found that the long-lived ^{3}MLCT state in this Ru complex was formed on the subpicosecond time scale[88]. We thus expect that the Ru N3 may also relax from the initially excited ^{1}MLCT state to its lowest-lying excited state, ^{3}MLCT, in the subpicosecond time scale. The observed new absorption peak at 5 ps is assigned to that of the ^{3}MLCT state. The formation and decay time of the excited ^{3}MLCT state, can be obtained from the kinetics measured at the peak positions for the ground and excited state. Shown in Fig. 7 are transient kinetics measured at the peaks of the transient spectra (2040 cm^{-1}) for a) Ru N3 in ethanol and b) RuN3 adsorbed on an Al_2O_3 thin film. The full circles in these figures are the experimental data and the solid lines are fits obtained by convolution of a single exponential rise function with the instrument response function.

For Ru N3 in ethanol solution, the rise time of the signal appears to be instrument response time limited. A fit with a 75 fs single exponential rise time (solid curve) is shown for comparison. Within the signal to noise ratio of the data, a satisfactory fit can be obtained for a single exponential rise time constant of <75 fs, which is considered as the upper limit of the rise time. For the Ru N3 adsorbed on Al_2O_3 film, because of the poor data quality and small number of data points on the rising edge of the data, the rise time of the signal

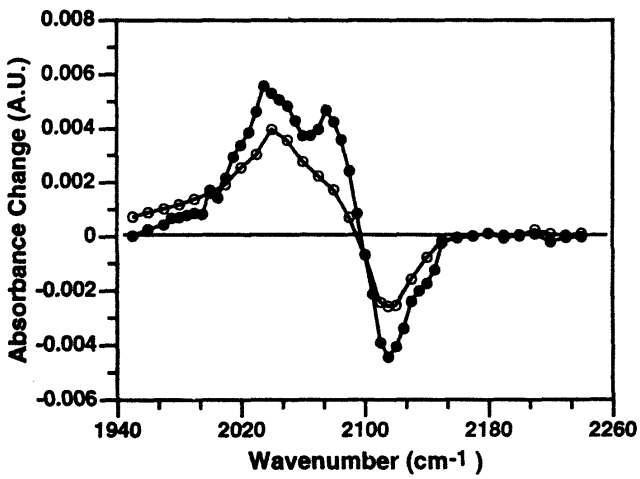

Fig. 6 Transient IR spectra of $Ru(dcbpy)_2(NCS)_2$ in ethanol (full circles) and adsorbed on nanocrystalline Al_2O_3 thin film (open circles) at 5 ps after 400 nm excitation.

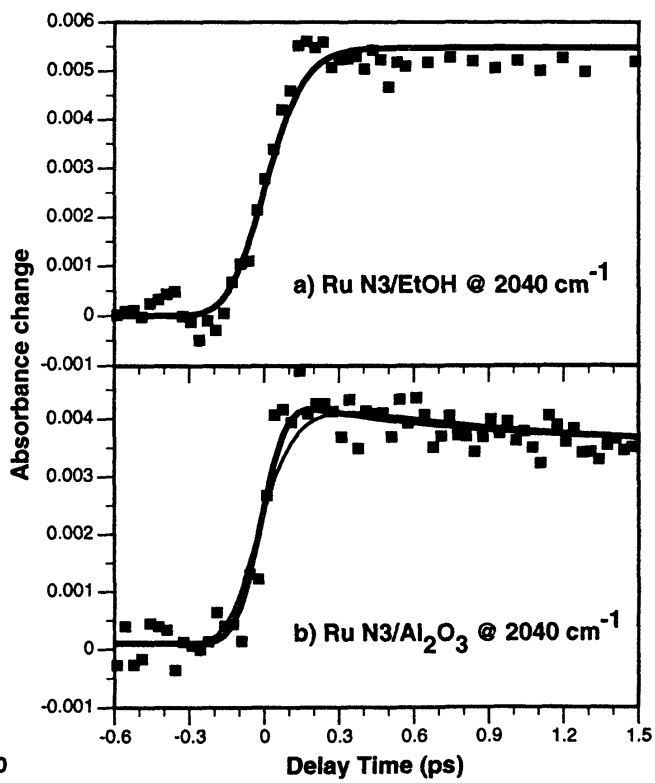

Fig. 7 Comparison of excited state formation kinetics probed at 2040 cm^{-1} for $Ru(dcbpy)_2(NCS)_2$ (a) in ethanol solution and (b) adsorbed in nanocrystalline Al_2O_3 thin film after 400 nm excitation. The solid lines represent fits to the data.

can not be accurately determined. Shown by the thick and thin solid lines are fits with single exponential rise time of 1 fs (to represent no rise time) and 100 fs. Within the signal to noise, satisfactory fits to the data can be obtained with a single exponential rise time of <100 fs. This result suggests that upon 400 nm excitation of ^{1}MLCT state, the molecules relax to their lowest lying triplet ^{3}MLCT state in less than 100 fs, consistent with the previous observation of an ultrafast formation time[88].

It should be pointed out that the above assignment of the ^{3}MLCT state formation time is based on the assumption that the CN stretching mode in the ^{3}MLCT state is different from that in the ^{1}MLCT state. To the best of our knowledge, we are not aware of any published results on the possible shift of CN stretching frequency in similar compounds. However, if the CN stretch frequencies are similar in the ^{1}MLCT and ^{3}MLCT states, the measured <100 fs rise time does not indicate the ^{3}MLCT state formation time.

The excited state decay kinetics at longer time scale for the Ru N3 on Al_2O_3 and Ru N3 in solution are shown in Fig. 8a (2115 cm^{-1}) and Fig. 8b (2040 cm^{-1}). The best fits to the data at 2115 cm^{-1} (the solid lines) for both samples are similar and show a > 1 ns recovery time, indicating negligible recovery of ground state molecules on the 1 ns time scale. The decay of the transient absorption at 2040 cm^{-1} is quite different for these two samples. For Ru N3 in solution, there is no noticeable decay, consistent with previous observation of a 59 ns lifetime of the ^{3}MLCT state[11]. For Ru N3 on Al_2O_3 the excited state absorption peak decays by about 50% by 1 ns. The decay kinetics can be fit by a bi-exponential decay function plus a long-lived component with the following time constants and initial amplitudes (in parenthesis): 3.5 ps (21%), 130 ps (26%) and >> 1 ns (53%), as shown in Fig. 8b. Since no ground state bleach recovery was observed, the decay of the excited state must produce a new species that is different from the ground state and lowest lying ^{3}MLCT state.

In this experiment, we are probing the IR absorption of the lowest lying excited state, not the fluorescence. Therefore, energy transfer between sensitizers would not cause any decay of the observed signal. One possibility of this new

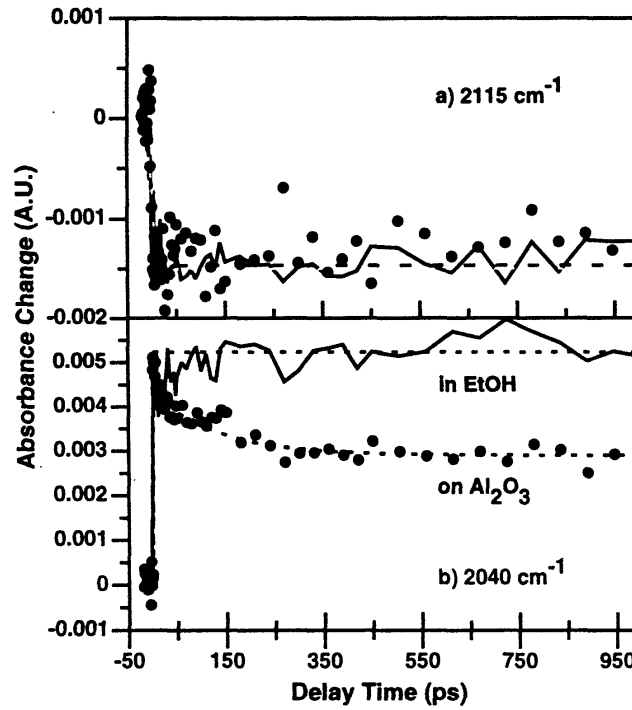

Fig. 8 Comparison of (a) excited state decay kinetics probed at 2040 cm^{-1} and (b) ground state recovery kinetics probed 2115 cm^{-1} for Ru(dcbpy)$_2$(NCS)$_2$ in ethanol solution (thin solid line) and adsorbed in nanocrystalline Al_2O_3 thin film (full circles) after 400 nm excitation. The dash lines are best fits to the data.

species corresponds to the injection of an electron from the dcbpy π^* orbital to the substrate. Although electron injection into the conduction band of Al_2O_3 is not possible in this large band gap material, a pathway involving electron transfer to surface states is possible. This pathway was invoked in a previous experiment of cresyl violet sensitized Al_2O_3[89], in which the fluorescence lifetime of the adsorbed dye at low coverage was found to be shorter compared to those in solution.

Electron Injection from Ru N3 to TiO_2

In order to unambiguously identify the injection step in Ru N3 dye sensitized TiO_2, we compare the transient IR absorption signal in the N3 sensitized TiO_2 films with naked TiO_2 films and Ru N3 sensitized Al_2O_3 thin films. Shown in Fig. 9 is one of such comparison of transient IR signals measured at 2040 cm^{-1} with 1.1 μJ of 400 nm excitation. It should be pointed out that the data shown in Figs. 6, 7, and 8 for Ru N3 sensitized Al_2O_3 were collected with about 7 times higher

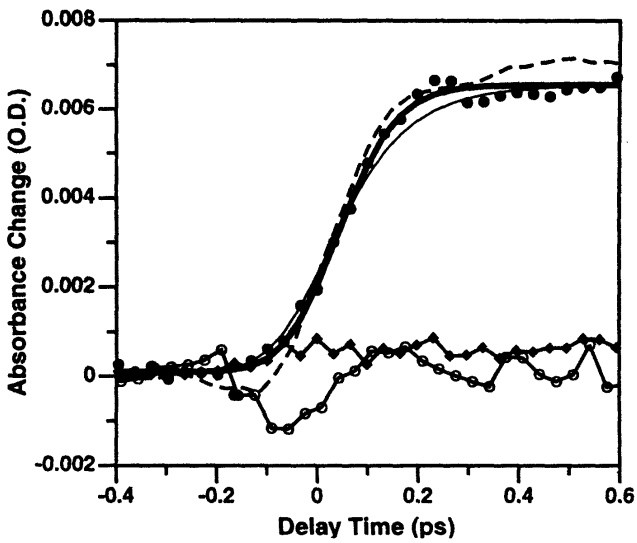

Fig. 9 Comparison of transient mid IR signal probed at 2040 cm^{-1} for Ru N3 sensitized TiO_2 (full circles), Ru N3 sensitized Al_2O_3 (open circles) and naked TiO_2 (full diamonds) thin films. The dash line shows an instrument response measure in a thin silicon wafer. The signal in Ru N3 sensitized TiO_2 thin films is assigned to injected electrons (see text). The best fit (thick solid line) to the data yields a 50 fs rise time, i.e. electron injection time. Also shown by the thin solid line is a fit with a 100 fs rise time.

pump power. At the reduced pump power of 1.1μJ, the amplitude of the signal due to Ru N3 vibrational spectral change can be estimated to be < 0.5 mOD, consistent with the negligible transient IR signal for Ru N3 sensitized Al_2O_3 indicated by the open circles in Fig. 9. The signal in the naked TiO_2 film is about 0.6 mOD, attributed to direct excitation of electrons near the conduction band edge and holes in the valence band[90]. Since both Ru N3 sensitized Al_2O_3 and naked TiO_2 films have negligible transient IR signals after 400 nm excitation, the observed 6 mOD absorption signal in the Ru N3 sensitized TiO_2 film can be attributed to electrons injected into TiO_2 from the sensitizer excited state.

Furthermore, the observed signal is very broad, present in all the mid IR wavelength probed so far, ranging from 1700 to 2400 cm^{-1}. This type of broad mid IR absorption signal can be attributed to injected electrons as discussed in earlier section.

Since the observed IR absorption for Ru N3 sensitized TiO_2 thin film shown in Fig. 9 is due to injected electrons, its rise time is the electron injection time from the sensitizer to TiO_2. The rise time of the data can be well fit by a single exponential rise function convoluted with the instrument response function. The best fit to the data at 2040 cm^{-1} yielded a 50 ± 25 fs rise as shown by the solid line. The error bar reflects a 50% increase of the χ^2 of the fit. The light line in Fig. 9 shows a similar curve with a 100 fs rise time, which can not give a satisfactory fit to the data. A similar rise time has been observed at probe wavelength in the 2000 to 2200 cm^{-1} region. We therefore report an average rise time of 50 ± 25 fs. In addition to this fast injection component, there appears to be a much smaller and slower rise component with time constant of 1.7 ± 0.5 ps[72]. We found that this second component was very sensitive to the sample condition. Its amplitude appeared to be bigger, ca. 16%, in freshly prepared samples and became smaller, ca. 5%, when the samples aged, although no noticeable difference could be observed from the static UV/Vis and FTIR spectra of the films. The exact origin of the second component is so far unknown. More experiments that carefully correlate sample preparation and transient kinetics will be carried out to resolve this issue. Our result clearly demonstrates that >84% of the electrons are injected in about 50 fs after the excitation of Ru N3 molecules at 400 nm.

It should be pointed out that the instrument response functions used in the deconvolution were determined in a thin silicon wafer, in which 400 nm excitation leads to instantaneous generation of electrons and holes. The Ru N3 sensitized TiO_2 films are highly porous consisting of interconnected nanoparticles of ca. 20 nm average diameter. Although negligible scattering of the probe IR beam is expected, some scattering of the 400 nm pump beam may be possible. This scattering process, if not negligible, may lengthen the effective instrument response function in these porous films compared to those measured in a silicon wafer. We have recently compared the instrument response function (IRF) determined from the rise time of the transient IR signal in a thin silicon wafer and unsensitized TiO_2 thin films, which were prepared under the same condition as those films used for the Ru N3 sensitized samples. It was found that observed IRF for the porous films

was about 20 fs longer than that in the silicon wafer. Since the amount of scattering in the Ru N3 sensitized film may be smaller due to its stronger absorption, the amount of correction for the IRF can be estimated to be < 20 fs, although the exact amount needed is unknown. A lengthened instrument response function due to scattering would require an even faster rise time to fit the data. Without a more accurate way of measuring the instrument response function in the porous film and because of the limited time resolution, we cannot exclude the possibility that the electron injection time is even faster than 50 ± 25 fs.

Comparison with Previous Works

Ultrafast electron injection dynamics in Ru N3 sensitized TiO_2 films have been studied by other groups[43,48]. Tachibana *et al.*[48], reported an almost equal amplitude biphasic injection process with time constants of <150 fs and 1.2 ps. Here the electron injection process was identified by measuring the apparent[91,92] transient spectrum in the 500 to 900 nm region of the oxidized form of N3 dye. The 1.2 ps rise component was directly measured at the peak of the oxidized dye absorption at 750 nm. The <150 fs injection component was inferred from the observation that the transient spectrum at 150 fs, the earliest time measured, was already half of the magnitude of the total spectral change at later time. The fast component appears to be consistent with our measured 50 fs injection time. However, the intensity of the second component with 50% of the total amplitude was much bigger than our 1.7± 0.5 ps (<16%) component. The origin for the discrepancy is so far unclear.

A more recent study of the same system in a UHV chamber[43] reported a different transient absorption in the visible and near IR region. The reason for the different transient spectra in UHV and solution is still a subject of further debate[91,92]. In this study a near IR absorption at 1100 nm was observed and assigned to injected electrons. Based on the rise time of the near IR signal, a <25 fs injection time was obtained. Our measured electron injection time is in agreement with the <25 fs injection time they reported[43]. However, it was found that similar near IR absorptions at 1500 nm could be observed under atmospheric conditions for Ru N3 on TiO_2, N3 in solution and N3 on ZrO_2 after excitation of the MLCT band[64]. The amplitudes of the latter two signals are about 70% of that for Ru N3 sensitized TiO_2 film under the same pump energy. This result indicates that under atmospheric conditions there may be significant absorption from the sensitizer excited state in the near IR region. More recently, Heimer and Heilweil also used mid-IR femtosecond IR spectroscopy to study the electron injection dynamics of Ru N3 and related Ru dye [Ru(5,5'-COCH2Ch3)2-2,2'-bippyridine)$(NCS)_2$] sensitized TiO_2 film. The Electron injection times in both films were found to be <350 fs[68]. It appears that all four measurements suggest that the electron injection from the MLCT state of Ru N3 sensitizer to TiO_2 can be on the 100 fs or faster time scale.

Identity of the Injecting State: Comparison with $Fe(dcbpy)_2(CN)_2$

The observed 50 fs injection time from Ru N3 to TiO_2 is on the same time scale of or faster than the intramolecular vibrational energy relaxation as well as intersystem crossing time of adsorbate molecules. The time scale of vibrational energy redistribution for large molecules in solution was often found to be on the order of 10s to 100s of femtosecond[93,94], although the exact time scale for Ru N3 molecules has yet to be determined. Electronic relaxation from the initially prepared Frank-Condon state to the long lived ^{3}MLCT state for $Ru(bpy)_3^{2+}$ in solution was found to occur on the 100 fs time scale[88]. Our measurement of the formation time of the CN stretch mode in the ^{3}MLCT excited state also yields a rise time of < 75 fs for Ru N3 in ethanol and adsorbed on Al_2O_3. If we assume a noticeable shift of CN stretching frequency from ^{1}MLCT state to the ^{3}MLCT state, the measured time suggests that the formation time of ^{3}MLCT state in Ru N3 is also occurring in the < 75 fs time scale. While it is possible that electron injection may occur in the same time scale or even prior to vibrational energy redistribution and intersystem crossing, as suggested in a recent paper[43], our data do not provide unambiguous evidence for the identity of the injecting state. Ongoing pump-wavelength dependent experiments may provide more insight into these important issues.

If electron injection can occur prior to excited state relaxation, one can also expect to observe

electron injection in $Fe(dcbpy)_2(CN)_2$ sensitized nanocrystalline TiO_2 films. In this system, the lowest lying excited state is the ligand field state, in which the excited electron populates the metal based d orbitals. Because of the poor orbital overlap between the d orbitals with the TiO_2 conduction band and unfavourable driving force, electron injection from the ligand field state to TiO_2 is expected to be unlikely[95] or much slower compared to injection from dcbpy π^* orbitals. In a recent study of solar cells based on $Fe(dcbpy)_2(CN)_2$ sensitized nanocrystalline TiO_2 film electrodes[95], photo-current was recorded when the cell was illuminated in the MLCT charge transfer band at wavelengths shorter than 500 nm. This result is interpreted as ultrafast electron injection from the excited MLCT state to TiO_2 prior to intersystem crossing from ^{1}MLCT state to lower lying ligand field states[95]. We have also conducted a preliminary investigation of the electron injection dynamics in $Fe(dcbpy)_2(CN)_2$ sensitized nanocrystalline TiO_2 thin films. Shown in Fig. 10 are transient IR signals in the $Fe(dcbpy)_2(CN)_2$ sensitized nanocrystalline TiO_2 thin film. Again, a broad IR absorption of injected electron was observed. The electron injection time appears to be faster than 100fs. However the amplitude of the transient signal in sensitized film relative to unsensitized film appears to be smaller compared to that of Ru N3 sensitized films, indicating a smaller injection efficiency for the $Fe(dcbpy)_2(SCN)_2$ sensitized film. This result is consistent with the reported smaller photon to current conversion efficiency in $Fe(dcbpy)_2(SCN)_2$ sensitized films[95]. Although much more work is needed to carefully compare these two different films, this study suggests that electron injection occurs on the same time scale of excited state electronic relaxation.

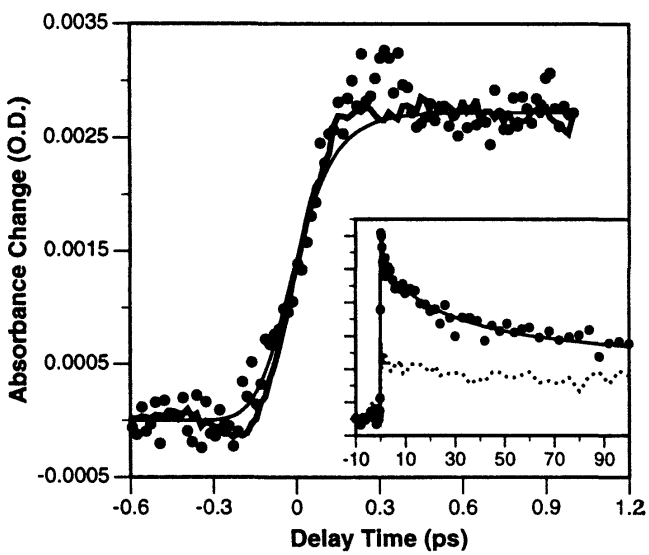

Fig. 10 Transient kinetics for $Fe(dcbpy)_2(CN)_2$ sensitized TiO_2 thin films probed at 2000 cm^{-1} after 400 nm excitation. The full circles are the data points, the thick solid line is the instrument response measured in a silicon wafer, and the thin solid line is a fit with 100 fs rise time. Shown in the inset is a comparison of mid IR absorption signal in sensitized (full circles) and unsensitized (dot line) TiO_2 thin films.

Related Ultrafast Electron Injection Dynamics

Many research groups have reported ultrafast electron injection from various sensitizers to TiO_2 in recent years. Using the fluorescence up-conversion technique, a forward electron injection time of 180± 50 fs was inferred from the fluorescence decay time of C-343 in a colloidal solution of sensitized TiO_2 nanoparticles in H_2O (with 5% acetone)[49]. More recent unpublished result from Castner *et al.* on C343 sensitizer TiO_2 nanoparticle colloidal solution suggested that the injection rate may be around 20 fs. These authors also reported a ca. 330 fs injection time in C343 sensitized ZnO nanoparticle colloids[56]. We have also measured the electron injection dynamics in C343 sensitized TiO_2 nanoparticles using transient IR absorption spectroscopy and reported a 125±25 fs electron injection time[69]. Electron injection dynamics in other dye sensitized TiO_2 nanoparticles have also been reported. Cherepy *et al.* measured a <100 fs electron injection time from anthocyanin dye sensitized TiO_2 nanoparticles. Martini *et al.*[46,97] have investigated electron injection dynamics in a series of anthracene dye sensitized TiO_2 nanoparticles. For 9-anthracene sensitized anatase TiO_2 nanoparticles, a < 200 fs electron injection time was observed, while for an amorphous form of TiO_2, a 1.5 ps electron injection time was measured. Burfeindt *et al.* have studied modified-perylene sensitized TiO_2 thin films in ultrahigh vacuum chamber. A 190 fs electron injection time was first reported[54] and a more recent measurement with improved time resolution yielded a 75 fs electron injection time[98]. Ultrafast electron injection on Oxazine sensitized

bulk SnS_2 crystal surface has also been studied by the fluorescence quenching technique. A 40 ± 20 fs electron injection time was inferred[50].

Mechanism of Ultrafast Electron Injection Process

Our measurement of Ru N3 sensitized TiO_2 thin film and C343 sensitized TiO_2 nanoparticle colloid as well as many similar measurements by other groups all reported ultrafast electron injection times on the 100 fs or faster time scale. In these dye sensitized systems, the sensitizer molecules attach strongly to the semiconductor. The exact reason for the ultrafast injection of electrons from the sensitizer to TiO_2 is so far unclear. In the case of Ru N3 dye sensitized TiO_2 films, a direct charge transfer transition from Ru to TiO_2 is not likely because of the lack of direct spectral overlap between Ru and TiO_2 orbitals. This notion is supported by the observation of only a small red shift of the Ru N3 absorption spectrum when adsorbed on TiO_2[19]. One possibility for the observed fast injection is a strong coupling of the dcbpy π^* orbital with TiO_2, leading to an adiabatic electron transfer from dcbpy to TiO_2. In this case, the optical transition corresponds to excitation from a Ru d orbital to a mixed state of dcbpy π^* and Ti 3d orbital. The electron transfer process would correspond to the motion of the initial wavepacket, which is prepared in the dcbpy side because of Frank-Condon overlap, to the TiO_2 side along the adiabatic surface. However, it is still unclear whether strong coupling is necessary for fast interfacial electron transfer processes from adsorbate to semiconductors, which have large density of states. According to Fermi's Golden rule, a large accepting state density in TiO_2 would also give rise to ultrafast injection time even when the coupling between dcbpy π^* orbital and TiO_2 is weak or intermediate. The extent of electronic coupling and origin of the ultrafast injection dynamics will be investigated in future experiments by systematically varying the coupling strength and density of accepting states.

5 Back ET from TiO_2 to $Fe(III)(CN)_6^{3-}$

While fast electron injection from sensitizer to semiconductor is essential for a high photon to current conversion efficiency, a slow recombination rate is also required. The back electron transfer in Ru N3 sensitized TiO_2 films has been determined to occur in the microsecond to millisecond time scale. The combined ultrafast electron injection and slow recombination is responsible for the almost 100% conversion efficiency for this sensitizer. In this section, we will focus on the back electron transfer dynamics from the semiconductor nanoparticles to the adsorbate. To achieve a more quantitative understanding of this process, we chose to study simple adsorbates, such as $Fe(II)(CN)_6^{4-}$ and SCN^-, that form charge transfer complexes with TiO_2 nanoparticles. In these complexes, a charge transfer transition can be directly excited with optical excitation, so the electronic coupling matrix elements of relevant potential energy surfaces and the Frank Condon active vibrational modes involved in the ET process can be determined experimentally[53,99-102]. These systems may serve as a good model system for quantitative analysis of interfacial ET. This type of treatment, which is common for intramolecular ET in homogeneous solutions[100-102], is rare for interfacial ET processes studied so far[53].

TiO_2 nanoparticles and $Fe(II)(CN)_6^{4-}$ molecules form charge transfer complexes under low pH[52,53,103-105] indicated by the formation of a new absorption band at 430 nm. Excitation of the charge transfer band leads to injection of electrons into TiO_2 and the formation of $Fe(III)(CN)_6^{3-}$[52,53]. The measured photon to current quantum efficiency was only 37% at 430 nm on a nanocrystalline anatase TiO_2 electrode[105], suggesting a substantial amount of back transfer of injected electrons from TiO_2 to ferric cyanide. Back ET to $Fe(III)(CN)_6^{3-}$ and related mono-substituted derivatives[52,105] has been well characterized on the sub-microsecond time scale. The detailed mechanisms of the back ET transfer dynamics in the sub-nanosecond regime have not been studied. In an effort to quantitatively understand interfacial ET dynamics, we have recently studied photoinduced electron transfer (ET) in $Fe(II)(CN)_6^{4-}$ sensitized TiO_2 nanoparticles in colloidal D_2O solution using sub-picosecond laser spectroscopy in the visible and in the mid infrared region. Non-single-exponential recombination kinetics were observed and the origin of this behaviour was investigated by modelling of the dependence of back ET rates on the spatial and energetic distribution of the trap states.

Structure of $Fe(II)(CN)_6^{4-}$ /TiO_2 Charge Transfer Complexes

Resonant Raman spectra of adsorbed $Fe(II)(CN)_6^{4-}$ on TiO_2 nanoparticles in colloidal solution at pH 1 to 3 show three peaks at 2058, 2072, and 2118 cm^{-1}[53]. These peaks were assigned to the trans(terminal), cis (radial) and bridging CN stretching modes of a singly CN bridged structure with C_{4v} symmetry[53]. Here, trans and cis are relative to the bridging CN. The IR spectrum of adsorbed $Fe(II)(CN)_6^{4-}$ on TiO_2 nanoparticles in D_2O solution has three CN stretching peaks at 2053, 2068 and 2093 cm^{-1}[71]. Under C_{4v} symmetry, CN stretching modes that are Raman allowed are also IR active[106], although the relative intensities of these modes are very different in the two spectra[107]. We therefore assigned the observed peaks in the IR spectra of the adsorbed $Fe(II)(CN)_6^{4-}$ in colloidal solution, at 2053, 2068 and 2093 cm^{-1}, to the terminal, cis and bridging CN stretching modes. The IR spectrum indicates that under our experimental conditions, the adsorbed $Fe(II)(CN)_6^{4-}$ on TiO_2 nanoparticles in the colloid and in the film has a singly CN bridged structure. It should be pointed out that adsorption of $Fe(II)(CN)_6^{4-}$ on metal electrodes can occur through singly, doubly or triply bridged structures depending on the pH of the solution and the size of the cations[106,108].

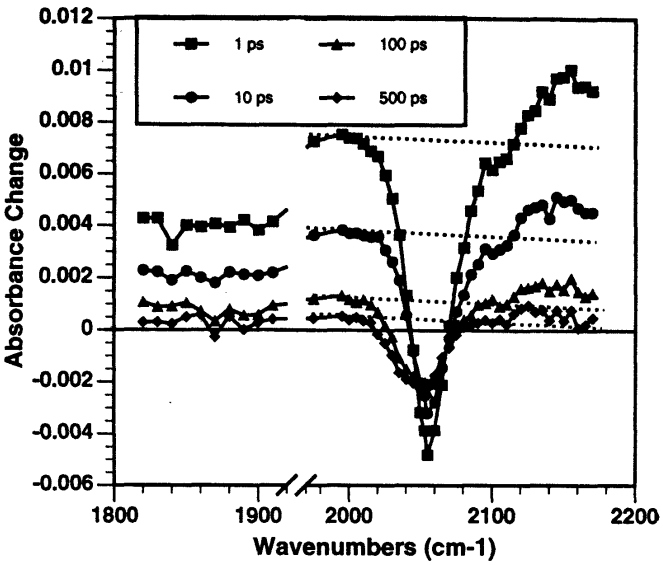

Fig. 11 Transient IR difference spectra of $Fe(II)(CN)_6^{4-}$ /TiO_2 in D_2O at 1, 10, 100 and 500 ps after 400 nm excitation. The spectrum at each delay time consists of a broad positive feature in the 2000 to 2150 cm^{-1} region (the dash line), a bleach of parent CN stretching modes at 2053 cm^{-1}, and a new positive peak centered around 2160 cm^{-1}. These features are assigned to injected electrons, depletion of $Fe(II)(CN)_6^{4-}$, and formation of $Fe(III)(CN)_6^{3-}$ respectively. The broad absorption feature of injected electrons can also be seen in the 1800-1900 cm^{-1} region.

Assignment of Transient IR Spectra

Shown in Fig. 11 are transient IR spectra of $Fe(CN)_6^{4-}$ sensitized TiO_2 colloid at 1, 10, 100 and 500 ps after 400 nm excitation. The spectrum at each delay time consists of a broad positive feature in the whole spectral region (the dashed lines), a bleach of parent CN stretching modes centered at *ca.* 2055 cm^{-1} and a new positive peak centered around 2160 cm^{-1}. These observed signals were shown to result from the excitation of the charge transfer complex, since blank experiments in unsensitized TiO_2/D_2O solution and $Fe(II)(CN)_6^{4-}$ solution yielded negligible signals. As demonstrated previously[52,105], excitation at the charge transfer band centered at 430 nm promotes electrons from $Fe(II)(CN)_6^{4-}$ to TiO_2. 400 nm excitation should also lead to electron injection to TiO_2, depletion of $Fe(II)(CN)_6^{4-}$ and formation of $Fe(III)(CN)_6^{3-}$. The depletion of $Fe(II)(CN)_6^{4-}$ is clearly shown by the observed bleach, relative to the dashed lines, in the 2030 to 2110 cm^{-1} region with a peak centered at about 2055 cm^{-1}. Free $Fe(III)(CN)_6^{3-}$ molecules in solution have a CN stretching band at 2115 cm^{-1} [103] and we have recently recorded a FTIR spectrum of adsorbed $Fe(III)(CN)_6^{3-}$ on TiO_2 , which has a main CN stretching band at 2153 cm^{-1}. We therefore assigned the absorption feature in the 2120 to 2180 cm^{-1} region with a center frequency at about 2160 cm^{-1} to the adsorbed $Fe(III)(CN)_6^{3-}$ created as a result of electron injection. The broad positive feature, indicated by the dashed line in Fig. 11, is assigned to the IR absorption of injected electrons inside TiO_2 nanoparticles[63], as discussed in section 3. This feature is more clearly shown in the 1800 to 1900 cm^{-1} region, where there is no overlap with adsorbate CN stretching bands.

Direct Electron Injection

To quantify the time evolution of the observed spectral features, kinetics at different wavelengths in the 1800 to 2150 cm^{-1} region were measured.

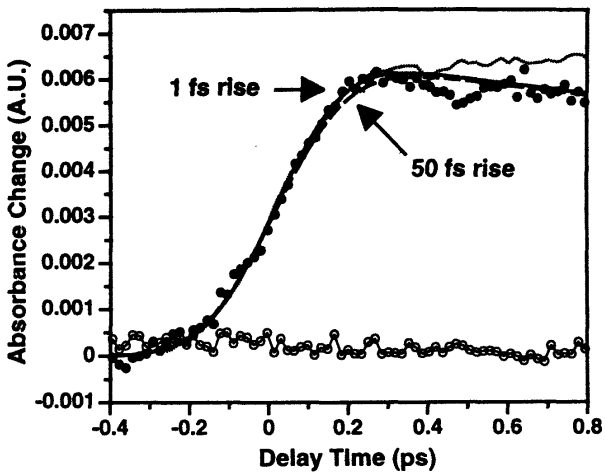

Fig. 12 Kinetics of the transient IR signal at 1850 cm^{-1} for $Fe(CN)_6^{4-}$ /TiO_2 colloidal solutions after 400 nm excitation (the full circles). The dotted line is the instrument response function measured in a nanocrystalline TiO_2 thin film. The solid lines is a fit of the data by convolution of the instrument response function with a 1 fs single exponential rise and the dashed line is a similar fit with a 50 fs rise time. The connected open circled are transient IR signals of unsensitized TiO_2 in D_2O under the same pump power.

Shown in Fig. 12 are kinetics measured at 1850 cm^{-1}. The dotted line is the instrument response measured in a naked TiO_2 thin film under the same pump power, which can be well represented by a Gaussian function with 320 fs FWHM. At 1850 (Fig. 12) and 1800 cm^{-1} (data not shown), the rise time of the signal appears to be instrument response time limited. Fits with single exponential rise functions yield satisfactory fits with time constants between 0 and 25 fs. A fit with time constant of 50 fs, shown by the dash line in Fig. 4, yields a noticeably worse fit to the data. Within the signal to noise of the data, no rise time is needed to fit the appearance of the IR signal. This instrument response time limited electron injection time is consistent with the charge transfer nature of the optical transition, which directly promotes an electron from a donor orbital in $Fe(II)(CN)_6^{4-}$ to an acceptor orbitals in TiO_2.

Back Electron Transfer Dynamics

The excitation of the direct electron transfer transition promotes an electron from the adsorbate molecules to the nanoparticle. The injected electron can relax within the nanoparticles and recombine with the adsorbate molecules. The bleach recovery in the CN stretch band is directly related the back electron transfer from the nanoparticle to the adsorbate and can be monitored independently.

The kinetics at 2053 cm^{-1} contain two contributions: the decay of the broad electron signal and the recovery of the CN stretching band. The kinetics for the CN stretch recovery alone can be obtained by subtracting the broad absorption signal indicated by the dash line in Fig. 11. Since the exact wavelength dependence of the amplitude of the signal is not known, the average of the kinetics at 2000 and 2115 cm^{-1} is used to describe the decay of the background at 2053 cm^{-1}. This approach assumes that the electron absorption signal depends linearly on wavenumbers in this narrow spectral region, which is a pretty good approximation because the electron absorption feature is very broad. Shown in Fig. 13 are the subtracted kinetics for the colloidal solution. The bleach recovery in the colloidal solution can be fit by a multi-exponential recovery with time constants of 3 ps (35%), 40 ps (30%) and > 1 ns (35%). To confirm the validity of the subtraction approach, the bleach recovery of the charge transfer band centered at 430 nm was also measured[71]. Similar multi-exponential recovery

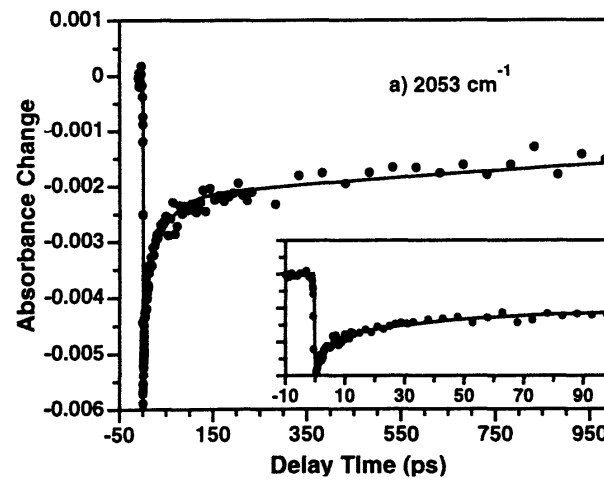

Fig. 13 Bleach recovery kinetics of the CN stretch mode for $Fe(II)(CN)_6^{4-}$ /TiO_2 colloidal solutions after 400 nm excitation. It was obtained by subtracting the kinetics at 2053 cm^{-1} by the averaged kinetics of 2000 and 2115 cm^{-1}. The bleach recovery is attributed to back electron transfer from TiO_2 to $Fe(III)(CN)_6^{3-}$. The solid line is the best three-exponential fit to the data. Displayed in the insert are the same kinetics in a shorter time scale.

kinetics were observed. The similarity between these two different measurements further confirms that the observed kinetics shown in Fig. 13 indeed describe the back ET dynamics.

The recovery of the CN bleach signal indicates the reformation of $Fe(II)(CN)_6^{4-}$ in its ground vibrational state. The observed recovery time constants can be directly related to back ET time, except for in the < 10s of picosecond time scale, in which vibration relaxation of hot $Fe(II)(CN)_6^{4-}$ formed after back ET may also contribute to the measured time. Ultrafast back ET is expected to produce vibrationally hot donor molecules as shown recently in intramolecular charge transfer complexes[107,109,110]. Unfortunately, the quality of the data is not adequate to allow more detailed analysis of vibrational relaxation dynamics. These dynamics, which contain information about back ET active vibrational modes, is of great interest to current ET research[107,109,110] and will be carefully examined in the future.

Back ET of $Fe(II)(CN)_6^{4-}$ sensitized TiO_2 in solution has been studied previously in the nanosecond to microsecond[52,105] time scale. In an earlier experiment with 20 ns time resolution[105], back ET was measured by monitoring the bleach recovery at 480 nm after 530 nm excitation. Back ET was found to be complete in 10 μs, with a half-life of 3 μs. More recently, in a similar measurement with 2 ns resolution[52], back ET time was found to be well represented by two components. The fast component, with about 50 % of the total amplitude, occurred with a time constant of 270 ns, and the slow non-exponential component appeared to be similar to that observed in the earlier measurement[105]. Combining all the results together, the back ET process is highly non-exponential, containing at least five different time constants, ranging from 3 ps to 3 μs. It is interesting to note that about 70% of the recombination occurs within 1 ns.

Origin of Non-Single-Exponential Back Electron Transfer Kinetics

The origin of the highly non-single-exponential nature of the back ET process has not been fully examined. Non-single-exponential recombination kinetics from TiO_2 to adsorbates have also been observed in $Ru(dcbpy)_2(SCN)_2$ sensitized TiO_2 thin film electrodes[48,111]. The back ET time was found to fall in the nanosecond to millisecond time scale and depend on bias-voltage of the electrode. There are at least three different reasons that can attribute to the nonexponential nanoparticle-to-adsorbate back electron transfer. First, there may be a large inhomogeneous distribution of adsorption sites. This leads to a distribution of donor-acceptor electronic coupling matrix elements, and therefore a distribution of the ET rates[12]. While an inhomogeneous distribution of adsorbing sites is possible, it is unlikely to be the only cause for the observed nonexponential ET process. If it is the dominating factor, then the observed back ET time, spanning 6 decades, suggests that the value for the square of the coupling matrix elements would need to vary by six order of magnitudes for different adsorbing sites. Secondly, unlike intramolecular ET, the injected electrons in the semiconductor nanoparticles can be localized at different parts of the nanoparticles. These different sites are located at varying distances away from the adsorbate molecule, ranging from a few to 50 A, the average diameter of the particles. This inhomogeneous distribution is further broadened by the inhomogeneous distribution of the particle sizes existing in the sample. If the trapped electrons recombine with the adsorbates through tunneling, the electronic coupling matrix element between the trap site and adsorption site is distance dependent, and the back ET reaction from these sites is expected to be non-single-exponential. For shallow trap sites, the trapped electrons may recombine with the adsorbate through diffusion encounter. In this case, the distribution in distance would lead to a distribution in the required diffusion time. Finally, in addition to the spatial distribution, these trap sites may also have very different energies, leading to a distribution of driving force and therefore the back ET rates[12]. The existence of trapping states with different energies has been observed in previous studies of TiO_2 thin film electrodes[90,112]. Similar trapping states can be expected for TiO_2 nanoparticles. The observed IR decay kinetics of electrons in TiO_2, as shown in Fig. 14 and discussed below, show electron trapping dynamics occurring in the picosecond to subnanosecond time scale in addition to back ET. Existence of relaxation processes that compete with electron transfer makes this an interesting and challenging system for study.

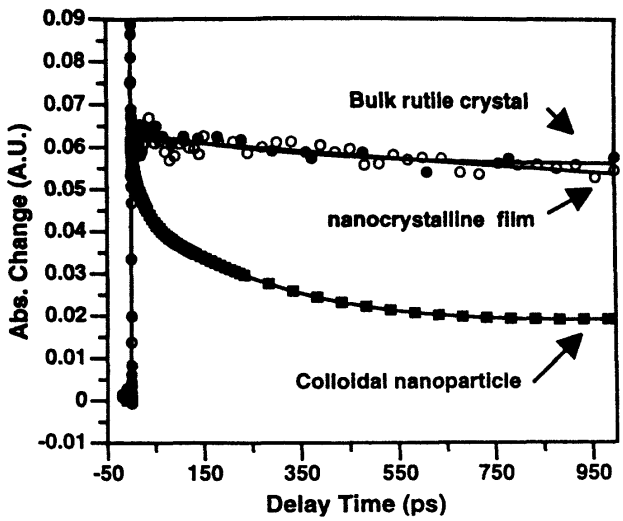

Fig. 14 Comparisons of decay kinetics probed in the mid IR region for electrons in three different TiO_2 materials: $Fe(II)(CN)_6^{4-}$ sensitized colloidal nanoparticles (connected filled squares), Ru N3 sensitized nanocrystalline thin films, and a bulk rutile crystal.

It appears that back ET from TiO_2 to $Fe(III)(CN)_6^{3-}$ involves electrons trapped in many different trapping sites, giving rise to highly non-exponential back ET dynamics. We also found recently that there was very little difference in the back electron transfer rate from TiO_2 to $Fe(III)(CN)_6^{3-}$ for particle sizes of about 3 and 11 nm[113]. This result indicates that the injected electrons are trapped at sites that are close to the adsorbates and are not homogeneously distributed over the entire particle. We are currently using the Marcus electron transfer rate theory and models of trapping site and energy distribution to model the nonexponential behaviour and the particle size independence of the back ET kinetics. The details of modelling will be communicated in future publications[113].

6 Relaxation Dynamics of Injected Electrons

The mid-IR absorbance of the injected electrons is proportional to the density of the injected electrons and their absorption cross section. The time dependence of the electron population reflects the electron transfer kinetics and the temporal evolution of the absorption cross section can be related to the electron relaxation processes within TiO_2. The observed decay of IR absorption signal contains the relaxation dynamics of electrons in TiO_2 in addition to the electron transfer dynamics discussed earlier. Shown in the Fig. 14 is a comparison of the electron relaxation dynamics in bulk rutile TiO_2 crystal, Ru N3 sensitized TiO_2 thin films and $Fe(CN)_6$ sensitized nanoparticles in solution.

For the bulk rutile crystal, the electrons and holes are generated through direct excitation of the bandgap transition. The decay of the signal within the first nanosecond is characterized by a pulse width limited decay (Fig. 5), and a subsequent slow decay of the amplitude with a time constant >> 1 ns. The fast decay can be attributed to fast cooling or recombination dynamics of the electrons. Subpicosecond electron cooling dynamics have been observed in many bulk semiconductor materials[114]. The slow subsequent decay suggest little carrier recombination or trapping dynamics in the ns time scale. For Ru N3 sensitized TiO_2 thin films, back ET time has been observed to occur in the μs to ms time scale. So there is no decay of population of the injected electrons in the < 1ns time scale. The observed decay of the IR signal can be attributed to the electron relaxation in the thin films only. The decay kinetics in different films vary slightly depending on film preparation.

For $Fe(II)(CN)_6^{4-}$ sensitized TiO_2 nanoparticles, at a probe wavelength that is far away from the CN bleach, such as 2000 cm^{-1}, the decay of the signal can be attributed to back electron transfer and electron trapping. If we assume a time dependent average cross section $\sigma(t)$ for the injected electrons as a result of trapping, the time-dependent mid IR absorption signal, $A(t)$, can be described by:

$$A(t) = \overline{\sigma}(t) * N_e(t)$$

where $N_e(t)$ is the population of injected electrons. The electron population is proportional to the amplitude of the CN bleach and can be determined independently as shown in Fig. 13. The average cross section of electrons can be obtained by dividing the observed absorbance change at 2000 cm^{-1} by the bleach recovery kinetics. The average cross section calculated according to this procedure is shown by connected squares in Fig. 14. It contains multi-exponential decay functions: 7 ps (8%), 35 ps (22%), 300 ps (40%), and >> 1ns (30%). This curve then represents the electron

relaxation dynamics in TiO_2 colloidal nanoparticles.

It is interesting to note that the trapping dynamics in the sensitized film and in a bulk TiO_2 crystal are similar[69,70], but they are much slower than those in colloidal nanoparticles[69-71]. Qualitatively, these decay kinetics can be attributed to relaxation of electrons from shallow trap to deep trap states. The trend in the electron relaxation rates is consistent with the trend of the density of trap states in these different crystalline TiO_2 materials. In principle, given the trap state density distribution and relaxation pathway, one can model quantitatively the electron relaxation kinetics. Unfortunately, the trap state density distribution is not well characterized and a detailed modelling of the decay kinetics has yet to be carried out.

7 Summary and Future Works

Electron transfer dynamics between semiconductor nanoparticles and molecular adsorbates have been studied using femtosecond mid-IR spectroscopy. With this technique, both the adsorbate vibrational spectral change and the mid IR absorption of injected electrons can be directly monitored. The direct observation of injected electrons allows for the unambiguous assignment of the electron transfer process.

The mid-IR absorption signal of electrons in or trapped below the conduction band were observed in the 5 μm region for bulk rutile TiO_2 crystal, nanocrystalline TiO_2 thin films, and colloidal nanoparticles. There appears to be very little spectral dependence in the 1950 to 2050 cm^{-1} region. The exact contribution of free carrier absorption, intraband transition and trapped electron absorption to the mid-IR absorption signal has yet to be determined. Ongoing measurements in a wider spectral region should allow a more detailed assignment of the observed signal. The time evolution of the absorption spectra will also provide insight into the relaxation dynamics of electrons in these materials. The trapping dynamics of electrons in nanocrystalline thin films and in a bulk single crystal are similar, showing very little decay on the < 1ns time scale. The trapping dynamics are much faster in colloidal nanoparticles, consistent with the trend of trap state densities in these materials.

Electron injection dynamics from adsorbate to TiO_2 were studied in Ru N3 dye sensitized nanocrystalline TiO_2 thin films. After the excitation of the ^{1}MLCT band of Ru N3 dye at 400 nm, electrons were excited from the Ru d orbital to the dcbpy π^* orbital. The subsequent electron injection time to TiO_2 was measured to be ca. 50 fs. The excited state dynamics of the Ru N3 dye in ethanol and adsorbed on Al_2O_3, a wide gap semiconductor, were also studied. The excited state relaxation from the initially excited singlet to the long-lived triplet MLCT state was found to occur on the < 100 fs time scale. This result indicates that electron injection from Ru N3 to TiO_2 may occur on a time scale that is the same as or faster than that for excited state relaxation.

Back electron transfer dynamics from TiO_2 to adsorbate were studied in $Fe(II)(CN)_6^{4-}$ sensitized TiO_2 colloidal solution. $Fe(II)(CN)_6^{4-}$ and TiO_2 forms a charge transfer complex, in which the excitation of the charge transfer band leads to direct promotion of an electron from $Fe(II)(CN)_6^{4-}$ to TiO_2. The appearance of the IR absorption signal for the injected electrons after 400 nm excitation was found to be instrument response time limited, consistent with the charge transfer nature of the optical transition. The injected electrons recombines with the adsorbate through a non-single-exponential process. A multi-exponential fit of the data yielded time constants ranging from 3ps to > 1 ns according to our measurement on the < 1ns time scale. Even longer recombination time constants of 270 ns[52] to 3 μs[105] were observed in previous studies in the nanosecond to microsecond time scale. The detailed origin of this nonexpoential process is being examined in our laboratory. Qualitatively, non-exponential recombination can be attributed to injected electrons in different trap sites. A quantitative model with spatial and energetic distribution of trapped electrons will be used to account for the non-single-exponential back ET dynamics.

Our study has shown that femtosecond mid IR spectroscopy can be used to study interfacial electron transfer between nanoparticles and molecular adsorbates. With this technique and complementary techniques in the visible region, we

can now start to systematically examine the dependence of interfacial ET rates on the properties of the adsorbates, nanoparticles, and interfacial environment. Quantitative comparison with interfacial electron transfer theory may now be possible since simple interfacial charge transfer complexes, such as $Fe(II)(CN)_6^{4-}/TiO_2$, can be studied and various parameters can be systematically changed. We are also extending this technique to study charge transfer dynamics in other nano-materials such as polymer/nanoparticle composites and nanoparticle arrays.

8 Acknowledgements

The authors would like to thank other collaborators of this project, R J Ellingson, S Ferrere and A J Nozik in NREL for their contribution in the Ru $N3/TiO_2$ study[64,70,72]. This work is supported in part by The Petroleum Research Fund, administered by the ACS, the Emory University Research Committee, and the National Science Foundation CAREER award under grant No. 9733796, and the Division of Chemical Sciences of the US Department of Energy.

References

1 R J D Miller, G L McLendon, A J Nozik, W Schmickler and F Willig *Surface Electron Transfer Processes* VCH Publishers Inc (1995)
2 A J Nozik and R Memming *J Phys Chem* **100** (1996) 13061
3 P V Kamat *Prog Reac Kinet* **19** (1994) 277
4 K I Jacobson and R E Jacobson *Imaging Systems* John Wiley & Sons New York (1976)
5 A Kay and M Gratzel *Solar Energy Materials and Solar Cells* **44** (1996) 99
6 N Serpone *Research On Chemical Intermediates* **20** (1994) 953
7 V L Colvin, M C Schlamp and A P Alivisatos *Nature* **370** (1994) 354
8 B Oregan and M Gratzel *Nature* **353** (1991) 737
9 A Hagfeldt and M Gratzel *Chem Rev* **95** (1995) 49
10 P V Kamat and D Meisel *Semiconductor Nanoclusters - Physical, Chemical and Catalytic Aspects* Elsevier Amsterdam **103** (1997)
11 M K Nazeeruddin, A Kay, I Rodicio, R Humphrybaker, E Muller, P Liska, N Vlachopoulos and M Gratzel *J Chem Soc* **115** (1993) 6382
12 R A Marcus and N Sutin *Biochem Biophys Acta* **811** (1985) 265
13 M D Newton and N Sutin *Ann Rev Phys Chem* **35** (1984) 437
14 P F Barbara, T J Meyer and M A Ratner *J Phys Chem* **100** (1996) 13148
15 R A Marcus *J Chem Phys* **43** (1965) 679
16 H Z Gerischer *Phys Chem Frankfurt* **26** (1960) 223
17 H Z Gerischer *Phys Chem Frankfurt* **27** (1961) 48
18 V G Levich and R R Dogonadze *Dokl Akad Nauk SSSR* **124** (1959) 123
19 N S Lewis *Ann Rev Phys Chem* **42** (1991) 543
20 *Laser Spectroscopy and Photochemistry on Metal Surface Part I & II* (Eds. H -L Dai and W Ho) World Scientific Publishing Co Singapore 5 (1995)
21 W Ho *Surf Sci* **300** (1994) 996
22 J P Culver, M Li, R M Hochstrasser and A G Yodh *Chem Phys* **205** (1996) 159
23 J P Culver, M Li, R M Hochstrasser and A G Yodh *Surf Sci* **368** (1996) 9
24 C M Wong, J D McNeill, K J Gaffney, N H Ge, A D Miller, S H Liu and C B Harris *Phys Chem* **B103** (1999) 282
25 C B Harris, N H Ge, R L Lingle, J D McNeill and C M Wong *Ann Rev Phys Chem* **48** (1997) 711
26 R Mcmming *Topics Curr Chem* **169** (1994) 105
27 J F Smalley, S W Feldberg, C E D Chidsey, M R Linford, M D Newton and Y P Liu *J Phys Chem* **99** (1995) 13141
28 S B Sachs, S P Dudek, R P Hsung, L R Sita, J F Smalley, M D Newton, S W Feldberg and C E D Chidsey *J Am Chem Soc* **119** (1997) 10563
29 Y Rosenwaks, B R Thacker, R K Ahrenkiel and A J Nozik *J Phys Chem* **96** (1992) 10096
30 Y Rosenwaks, B R Thacker, A J Nozik, R J Ellingson, K C Burr and C L Tang *J Phys Chem* **98** (1994) 2739
31 G N Ryba, C N Kenyon and N S Lewis *J Phys Chem* **97** (1993) 13814
32 K B Eisenthal *Chem Rev* **96** (1996) 1343
33 Y R Shen *Solid St Commun* **102** (1997) 221
34 G L Richmond *Anal Chem* **69** (1997) A536
35 J M Lanzafame, S Palese, D Wang, R J D Miller and A A Muenter *J Phys Chem* **98** (1994) 11020
36 A P Alivisatos *J Phys Chem* **100** (1996) 13226
37 D J Norris and M G Bawendi *Phys Rev B-Cond Matter* **53** (1996) 16338
38 B A Smith, D M Waters, A E Faulharber, M A Kreger, T W Roberti and J Z Zhang *J Sol-Gel Sci Tech* **9** (1997) 1
39 J Z Zhang *Acc Chem Res* **30** (1997) 423
40 V F Kamalov, R Little, S L Logunov and M El-Sayed *J Phys Chem* **100** (1996) 6381
41 J H Hodak, I Martini and G V Hartland *J Phys Chem* **B102** (1998) 6958
42 T Heimer and E J Heilweil *J Phys Chem* **B101** (1997) 10990
43 T Hannappel, B Burfeindt, W Storck and F Willig *J Phys Chem* **B101** (1997) 6799
44 A J Nozik, R J Ellingson, A Meieer, S Kocha, B B Smith and M Hanna *Proc Twenty-first DOE Solar Photochem Res Conf* (1997) 9
45 I Martini, G V Hartland and P V Kamat *J Phys Chem* **B101** (1997) 4826
46 I Martini, J H Hodak, G V Hartland and P V Kamat *J Chem Phys* **107** (1997) 8064

47 N J Cherepy, G P Smestad, M Gratzel and J Z Zhang *J Phys Chem* **101** (1997) 9342

48 Y Tachibana, J E Moser, M Gratzel, D R Klug and J R Durrant *J Phys Chem* **100** (1996) 20056

49 J M Rehm, G L McLendon, Y Nagasawa, K Yoshihara, J Moser and M Gratzel *J Phys Chem* **100** (1996) 9577

50 J M Lanzafame, R J D Miller, A Muenter and B Parkinson *J Phys Chem* **96** (1992) 2820

51 R Eichberger and F Willig *Chem Phys* **141** (1990) 159

52 H Lu, J N Prieskorn and J T Hupp *J Am Chem Soc* **115** (1993) 4927

53 R L Blackbourn, C S Johnson and J T Hupp *J Am Chem Soc* **113** (1991) 1060

54 B Burfeindt, T Hannapel, W Storck and F Willig *J Phys Chem* **100** (1996) 16463

55 D Liu, R W Fessenden, G L Hug and P V Kamat *J Phys Chem* **B101** (1997) 2583

56 K Murakoshi, S Yanagida, M Capel and J E W Castner *Interfacial Electron Transfer Dynamics of Photosensitized Zinc Oxide Nanoclusters ACS Symposium Series* (1997) 679

57 D Liu, P V Kamat, K G Thomas, K J Thomas, S Das and M V George *J Chem Phys* **106** (1997) 6404

58 R W Fessenden and P V Kamat *J Phys Chem* **99** (1995) 12902

59 J C Owrutsky, D Raftery and R M Hochstrasser *Ann Rev Phys Chem* **45** (1994) 519

60 M A Cavicchia and R R Alfano *Phys Rev B-Cond Matt* **51** (1995) 9629

61 M Woemer, T Elsaesser and W Kaiser *Phys Rev* **B45** (1992) 8378

62 K Faist, F Capasso, D L Sivco, C Sirtori, A L Hutchinson and A Y Cho *Science* **264** (1994) 553

63 J I Pankove *Optical Processes in Semiconductors* Dover New York (1975)

64 R J Ellingson, J B Asbury, S Ferrere, H N Ghosh, T Lian and A J Nozik *J Phys Chem* **B102** (1998) 6455

65 R McElroy and K Wynne *Phys Rev Lett* **79** (1997) 3078

66 D S Venables and C A Schmuttenmaer *J Chem Phys* **108** (1998) 4935

67 G Haran, W D Sun, K Wynne and R M Hochstrasser *Chem Phys Lett* **274** (1997) 365

68 T Heimer and E J Heilweil Measuring Ultrafast Sensitizer-TiO_2 Electron Dynamics with Mid-Infrared Spectroscopy *Ultrafast Phenomena* **XI** (1998)

69 H N Ghosh, J B Asbury and T Lian *J Phys Chem* **B102** (1998) 6482

70 J B Asbury, H N Ghosh, R J Ellingson, S Ferrere, A J Nozik and T Lian Femtosecond IR Study of Ru Dye Sensitized Nanocrystalline TiO_2 Thin Films: Ultrafast Electron Injection and Relaxation Dynamics *Ultrafast Phenomena* **XI** (1998)

71 H N Ghosh, J B Asbury, Y Weng and T Lian *J Phys Chem* **B102** (1998) (in press)

72 J B Asbury, R J Ellingson, H N Ghosh, S Ferrere, A J Nozik and T Lian *J Phys Chem* **B103** (1999) (in press)

73 H N Ghosh, J B Asbury and T Lian (unpublished results)

74 D Bahnemann, A Henglein, J Lilie and L Spanhel *J Phys Chem* **88** (1984) 709

75 R G Breckenridge and W R Hosler *Phys Rev* **91** (1953) 793

76 Enea, J Moser and M Gratzel *Electroanal Chem* **259** (1989) 59

77 S A Haque, Y Tachibana, D R Klug and J R Durrant *J Phys Chem* **B102** (1998) 1745

78 S G Yan and J T Hupp *J Phys Chem* **B101** (1997) 1493

79 S G Yan and J T Hupp *J Phys Chem* **100** (1996) 17

80 A Zaban, S Ferrere and B A Gregg *J Phys Chem* **B102** (1998) 452

81 A Zaban, S Ferrere, J Sprague and B A Gregg *J Phys Chem* **B101** (1997) 55

82 K Vinodgopal, X Hua, R L Dahlgren, A G Lappin, L K Patterson and P V Kamat *J Phys Chem* **99** (1995) 10883

83 R Argazzi, C A Bignozzi, T A Heimer, F N Castellano and G J Meyer *J Phys Chem* **B101** (1997) 2591

84 T A Heimer and G J Meyer *J Luminescence* **70** (1996) 468

85 T A Heimer, S T Darcangelis, F Farzad, J M Stipkala and G J Meyer *J Inorg Chem* **35** (1996) 5319

86 W E Ford and M A J Rodgers *J Phys Chem* **98** (1994) 3822

87 V E Henrich and P A Cox *The Surface of Metal Oxides* Cambridge University Press (1994)

88 N H Damrauer, G Cerullo, A Yeh, T R Boussie, C V Shank and J K McCusker *Science* **275** (1997) 54

89 R Kietzmann, F Willig, H Weller, R Vogel, D N Nath, R Eichberger and P Liska and J Lehnert *Molecul Cryst Liqui Cryst* **194** (1991) 169

90 G Rothenberger, D Fitzmaurice and M Gratzel *J Phys Chem* **96** (1992) 5983

91 T Hannappel, C Zimmermann, B Meissner, B Burfeindt, W Storck and F Willig. *J Phys Chem* **B102** (1998) 3651

92 J E Moser, D Noukakis, U Bach, Y Tachibana, D Klug, J R Durrant, R Humphry-Baker and M Gratzel *J Phys Chem* **B102** (1998) 3649

93 A Mokhtari, A Chebira and J Chesnoy *J Opt Sci Am* **B7** (1990) 1551

94 F Laermer and T Elsaesser *J Opt Soc Am* **B7** (1990) 1604

95 S Ferrere and B A Gregg *J Am Chem Soc* **120** (1998) 843

97 I Martini, J H Hodak and G V Hartland *J Phys Chem* **B102** (1998) 607

98 B Burfeindt, S Ramakrishna, C Zimmermann, B Meissner, T Hannappel, W Storck and F Willig *Ultrafasrt Phenomena* **XI** (1998)

99 N S Hush *Electrochimica Acta* **13** (1968) 1005

100 A B Myers *Chem Phys* **180** (1994) 215

101 J T Hupp, Y H Dong, R L Blackbourn and H Lu *J Phys Chem* **97** (1993) 3278

102 W Klaas and R M Hochstrasser *Advan Chem Phys* (1997) (In press)

103 J Desilvestro, S Pons, E Vrachnou and M Gratzel *J Electroanal Chem* **246** (1988) 411

104 E M G Vrachnou and A J McEvoy *J Electroanal Chem* **258** (1989) 193

105 E Vrachnou, N Vlachopoulos and M Gratzel *J Chem Soc Chem Commun* (1987) 868

106 C Korzeniewski, M W Severson, P P Schmidt, S Pons and M Fleischmann *J Phys Chem* **91** (1987) 5568

107 C Wang and G C Walker *J Am Chem Soc* (1998) (Submitted)

108 C M Pharr and P R Griffiths *Anal Chem* **69** (1997) 4665
109 S K Doom, R B Dyer, P O Stoutland and W H Woodruff *J Am Chem Soc* **115** (1993) 6398
110 K G Spears, X N Wen and R H Zhang *J Phys Chem* **100** (1996) 10206
111 S A Haque, Y Tachibana, D R Klug and J R Durrant *J Phys Chem* **B102** (1998)
112 A Kay, R Humphrybaker and M Gratzel *J Phys Chem* **98** (1994) 952
113 Y Weng, H Ghosh, J B Asbury, Y Wang and T Lian (mss in preparation)
114 J Shah *Ultrafast Spectroscopy of Semiconductors and Semiconductor Nanostructures* Springerverlag **115** (1996)